Aggregation of Gold Nanorods for in-liquid quantitative SERS detection of BSA

Antonino Foti[1,2], Barabara Fazio[1], Cristiano D'Andrea[1,3], Elena Messina[1], Alessia Irrera[1], Maria Grazia Donato[1], Valentina Villari[1], Norberto Micali[1], Onofrio M. Maragò[1], Pietro G. Gucciardi[1]

[1] *CNR, Istituto per i Processi Chimico-Fisici, Viale F. Stagno DAlcontres 37, Messina, I-98158, Italy*
[2] *Dipartimento di Scienze Matematiche e Informatiche, Scienze Fisiche e Scienze della Terra, viale F. Stagno d'Alcontres 31, Messina, Italy*
[3] *MATIS IMM - CNR, via S. Sofia 64, 95123 Catania, Italy*

E-mail: foti@ipcf.cnr.it, anfoti@unime.it

Abstract

Molecular detection in liquid environment exploiting Surface Enhanced Raman Spectroscopy (SERS) is usually based on chemically-driven aggregation of metal nanoparticles in presence of the target molecules. Such strategies allow the formation of SERS-active clusters that efficiently embed the molecule at the hot spots of the nanoparticles and enhance its Raman scattering by orders of magnitude. Optical forces can play an important role in this field because of the possibility of contactless manipulation of plasmonic nanoparticles in order to create SERS active sites in liquid. Here we report on a novel scheme that exploits the radiation pressure to locally push gold nanorods and induce their aggregation in buffered solutions of biomolecules, achieving biomolecular SERS detection at almost neutral pH. The sensor is applied to detect non-resonant amino acids and proteins, namely Bovine Serum Albumin (BSA), reaching detection limits in the μg/mL range. The sensor also shows a predictable intensity variation as a function of the concentration, allowing for a quantitative study of the solutions.

Keywords: SERS biosensor, in-liquid detection, BSA.

Introduction

Surface-enhanced Raman scattering (SERS) [1–3] takes advantage of the huge electromagnetic field enhancement (10^4 - 10^8) provided by localized surface plasmon resonances (LSPR) in metal nanoparticles (NPs)[4]. SERS has shown enormous application potentials in label-free detection of biomolecules [5–7] and proteins [8, 9] adding to standard surface plasmon resonance sensors the spectral information, useful to get insights on the conformation and structure of the biomolecules [10].

On the other hand, label-free SERS detection of proteins in liquid environment has turned out to be a challenge, due to the difficulty to efficiently induce SERS-active aggregates in a solution containing biomolecules without altering their functionalities. The addition of NPs aggregates to protein solutions paved the way to quantitative SERS of uric acid in human serum with limits of detection (LOD) $\sim$ 240 μM (equivalent to 40 μg/mL)[11]. An effective strategy to improve the sensitivity is to induce the NPs aggregation in presence of the target protein, e.g. via addition of acidified sulfate [12]. This yields SERS-active colloid-protein complexes in which the biomolecule is located at the NPs interstices (hot spots) allowing for detection of non-resonant proteins at concentrations down to 5 μg/mL (Lysozyme, Lys) [11].

Optical forces [13] can play an important role in this context, enabling the formation of efficient SERS hot spots in a controlled, contactless way [14, 15]. Light exerts forces and torques on metal NPs, enhanced by the plasmon resonances [16–18]. When the energy of the laser field is far-off the LSPR, optical forces by focused laser beams are dominated by the gradient force [14, 18] and can either attract [19–21] or repel [17, 22] metal NPs from high field intensity regions, permitting to either trap metal NPs in the spot of a tightly focused Gaussian beam or push them in the hollow core of a Laguerre-Gauss beam. Instead, when the light is nearly-resonant with the particle LSPR, optical forces are dominated by radiation pressure [14] and can be used to push metal NPs along the beam optical axis onto a substrate [23, 24]. Pioneering experiments have shown that trapping forces permit to bring together individual metal NPs and create SERS-active dimers [25]. It is also possible to trap gold colloids aggregated in presence of BSA and detect the enhanced Raman scat-

tering of the protein [26].

The possibility to exploit the radiation pressure to selectively push and aggregate metal NPs for SERS detection, remains largely unexplored. This approach represents a step forward in the development of SERS-based molecular sensors in liquid, since it allows one to use lasers with a broader wavelength range (no more limited by the LSPR of the NPs), it enables the controlled local spotting of metal nanoparticles on surfaces or even into living cells [24] for local SERS analysis. Here we focus on a novel label-free, all-optical SERS sensor for biomolecular detection in liquid (in LIQUId SERS sensOR, hereinafter LIQUISOR) that exploits the radiation pressure to push gold nanorods on a surface and form SERS-active aggregates in buffered solutions of amino acids and proteins . This methodology allows to detect Phenylalanine (Phe), Bovine Serum Albumin (BSA) and Lysozyme (Lys) at concentrations down to few μg/mL (100nM) with enhancement factors of about 10^5 [27]. In this work we show the possibility to use the LIQUISOR method to perform a quantitative analysis in order to estimate the concentration of BSA inside buffered solutions looking at the SERS intensity of the enhanced vibrational modes of the protein.

Materials and Method

Nanorods

Commercial gold nanorods (35nm diameter, 90 nm length) are purchased from Nanopartz and used as received. They are dispersed in deionized (DI) water at a concentration of 0.05 mg/ml, equivalent to ca. 310^7 rods/μL; the solution contains $< 0.1\%$ ascorbic acid and $< 0.1\%$ Cetyltrimethylammonium bromide (CTAB) surfactant preventing spontaneous re-aggregation. The solution varies between pH = 3-4. The capped rods have a positive ζ-potential (+40 mV).

Chemicals and sample preparation

Bovine Serum Albumin was purchased from Aldrich in lyophilized powder state. Protein buffered solutions at various concentrations are prepared by mixing the suitable amount of protein powder with a 200 mM of Phosphate Buffer Solution (pH 7.2). PBS is prepared by dissolving Na_2HPO_4 (14.94 g) and NaH_2PO_4 (5.06g) in 200mL of DI water. Following this procedure we prepared samples containing BSA at concentrations of 10^{-4} - 10^{-6} M. The NRs-proteins solutions are prepared by mixing the nanorods with the proteins dissolved in PBS in a volume ratio of 1:7 v/v, small enough to preserve the neutral pH (7.2) of the biomolecules solutions. All the solutions are prepared and used at room temperature.

Experimental setup

The LIQUISOR detection is carried out with a LabRam HR800 Raman confocal Micro-Spectrometer (Horiba Jobin Yvon) coupled to a He-Ne laser (λ = 632.8 nm); the laser beam is focused by means of a 100X (Olympus M-Plan, NA = 0.90, WD = 210 μm) microscope objective mounted on a Olympus BX41-microscope working in a straight configuration. The laser power on the sample is 5.0 mW, enough to apply a sufficient radiation pressure on the nanorods for process activation. 75 μL of the biomolecule-NRs solution is pipetted into a glass microcell consisting of microscope slides with hemispherical cavities (15 - 18 mm dia., 0.5 - 0.8 mm depth). The microcells are covered with glass coverslips 170 μm thick purchased from Forlab. The SERS signal of the BIO-NRCs is collected via the same illumination objective, in backscattering, dispersed by a 600 l/mm grating and detected through a Peltier-cooled silicon CCD (Synapse, Horiba Jobin Yvon). Spectra are typically acquired with integration times from seconds to tens of seconds.

Results and Discussion

The working principle of the LIQUISOR is the following: Gold nanorods are added to a solution of BSA dissolved in phosphate buffer saline. The mixture is enclosed in a glass microcell and placed under a Raman micro-spectrometer. Upon mixing, the biomolecules bind to the NRs [28], due to the interplay between the electrostatic interaction with the positively charged CTAB bilayer of molecules surrounding the NRs [29]. This yields the formation of biomolecule-NRs complexes (BIO-NRCs). Operation of the LIQUISOR is carried out by focusing the laser spot inside the microcell, in proximity of the bottom surface. To foster the aggregation, in fact, the NRs must be spatially confined in a region of few tens of microns. This is achieved by positioning the laser spot as close as possible to the rim of the hemispherical microcell, in the limited free space between the microcell sidewalls and the coverslip. Such process enables the dynamic accumulation of the NRs on the bottom surface of the microcell, in a zone around the laser focus, where the NRs stick and accumulate, forming aggregates that grow with time, reaching the size of several microns (Figure 1).

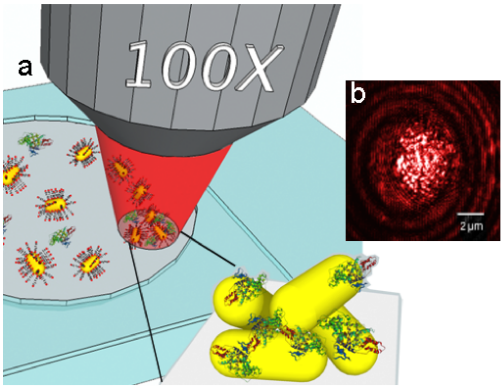

Figure 1: *(a) Detection scheme of the Liquisor. Laser beam ($\lambda = 632.8nm$) is focused on a micron scale spot in liquid (P = 5.0mW), close to the sidewalls of the microcell in order to foster the Bio-NanoRods complexes (BIO-NRCs) accumulation with the consequent formation of a SERS active aggregate whose hot-spots are filled with proteins. (b) Laser scattering image shows that the aggregate size can reach the micron size.*

Acquiring consecutive SERS spectra during the BSA-NRs optical aggregation highlights the aggregation dynamics of the LIQUISOR showed in Figure 2. The process follows two different time scales. The onset of the BIO-NRCs formation is observed after few seconds from irradiation when the first early stage aggregates is crated within the laser focal spot. The aggregates stick on the cell sidewall and stabilize in the next few tens of seconds (20 - 60 sec), producing a clear SERS signal of the biomolecule.

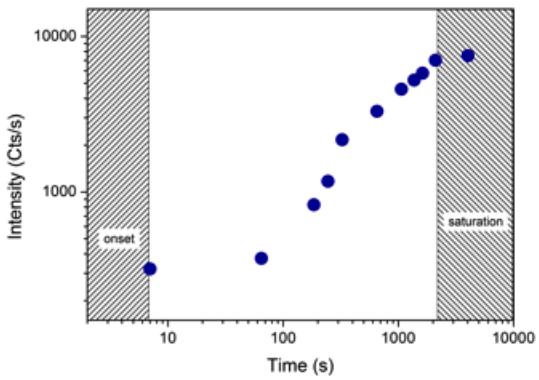

Figure 2: *SERS intensity of the phenylalanine ring breathing mode at 1005* cm^{-1} *as a function of time during the BIO-NRCs aggregation when the protein concentration is 0.1 mM.*

On longer time scales (1 - 10 min) the aggregate repeatedly increases its dimensions due to the capture of further BSA-NRs complexes, adding up proteins and hot spots sites, further enhancing the SERS signal. The process keeps going with time, producing aggregates that can reach the size of several microns, due to the fact that the optical forces push the NRs all around the laser spot. The SERS signal, however, saturates typically after some tens of minutes (10 - 40 min), i.e. when the NRs-protein complexes have totally filled the laser focal volume. NRs laying outside the focal spot do not contribute to the detected SERS signal, due to the confocal arrangement of the detection system [27].

In order to create a calibration curve for our biosensor based on the LIQUISOR methodology, we monitor the aggregation dynamics as a function of protein concentration in PBS solutions, from 0.1 mM down to 1 μM. We consider for our analysis the intensity after saturation of the Phenylalanine ring-breathing mode at 1005 cm^{-1} after background subtraction. The plot showed in Figure 3 clearly points out that SERS intensity at saturation grows as a function of the concentration in a very predictable way, permitting one to perform quantitative analysis on unknown concentrations of BSA solutions.

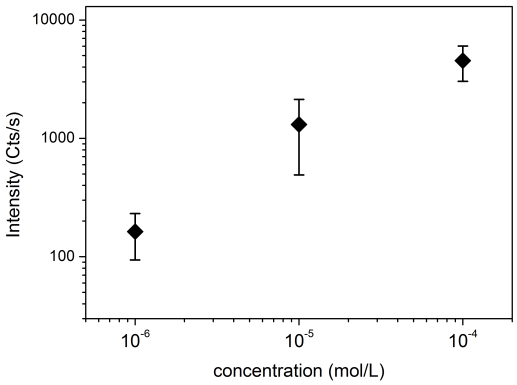

Figure 3: *SERS intensity, after saturation, of the BSA phenylalanine ring breathing mode at 1005* cm^{-1} *as a function of the concentration.*

Conclusions

In conclusion, we have demonstrated that the LIQUISOR methodology is suitable to perform quantitative detection of BSA of concentration down to the μM range, with the possibility to reach lower concentrations down to at least 0.1 μM. This approach can be also tailored to other proteins of high biomedical interest such as Lysozyme, whose raised levels in plasma may be a useful biomarker of atherosclerotic cardiovascular disease and response to therapy [30] or the manganese super oxide dismutase (Mn-SOD), a liver cancer biomarker [31]. Specificity can potentially be added to the LIQUISOR by using NPs

functionalized with aptamers or antibodies capable to capture the target biomolecules in liquid, thus enabling specific detection of pathology biomarkers in liquid environment.

Acknowledgement

We acknowledge M. A. Iatì, R. Saija, E. Di Fabrizio, M. Lamy de La Chepelle for fruitful discussions. We greatly acknowledge financial support from MIUR under projects PRIN 2008J858Y7 "Plasmonics in self-assembled nanostructures", PON01 01322 PANREX, and PAC02L3 00087 SOCIAL-NANO, from the EU under project FP7-HEALTH-F5-2009-241818-NANOANTENNA, and from the COST action MP1302 "Nanospectroscopy" and MPNS1205 "Adavances in Optofluidics: Integration of Optical Control and Photonics with Microfluidics".

References

[1] Kneipp, K.; Moskovits, M.; Kneipp, H. *Surface Enhanced Raman Scattering*, Springer, New York, 2006.

[2] Le Ru, E.; Etchegoin, P.: *Principles of Surface Enhanced Raman Spectroscopy*, Elsevier, Amsterdam, 2009.

[3] Lamy de La Chapelle M.; Lidgi-Guigui N.; Gucciardi P. G.; *Handbook of Enhanced Spectroscopy*, Pan Stanford Publishing Pte Ltd, 2015.

[4] LeRu, E.; Meyer, M.; Etchegoin, P.G.: *J. Phys. Chem. C* , **111**, 2007, p. 13794–13803.

[5] Cao, Y.W.C.; Jin, R.C.; Mirkin, C.A.: *Science*, **297**, 2002, p. 1536–1540.

[6] Bantz, K.C. et al.: *Phys. Chem. Chem. Phys.*, **13**, 2011, p. 11551–11567.

[7] Xie, W.; Schlücker: *Phys. Chem. Chem. Phys.*, **15**, 2013, p. 5329–5344.

[8] Han, X.X.; Zhao, B.; Ozaki, Y.: *Anal. Bioanal. Chem.*, **394**, 2009, 1719–1727.

[9] Shanmukh, S. et al.: *Nano Lett.*, **6**, 2006, p. 2630–2636.

[10] Nakamura, K.; Era, S. et al.: *FEBS Lett.*, **417**, 1997, p 375–378.

[11] Zakel, S., et al.: *Analyst*, **136**, 2011, p 3956–3961.

[12] Le Ru, E.; Etchegoin, P.: *Chem. Phys. Lett.*, **423**, 2006, p. 63–66.

[13] Ashkin, A.: *Phys. Rev. Lett.*, **24**, 1970, p. 156.

[14] Lehmuskero, A.; Johansson, P. et al.: *ACS Nano*, **9** 2015, 3453-3469.

[15] Maragò, O. M. et al.: *Nat. Nanotechnol.*, **8**, 2013, p 807–819.

[16] Hongxing, X.; Käll, M.: *Phys. Rev. Lett.*, **89**, 2002, p. 246802.

[17] Messina, E., et al.:*ACS Nano*, **5**, 2011, p. 905–913.

[18] Messina, E., et al.: *Opt. Express*, **23**, 2015, p. 8720–8730.

[19] Svoboda, K.; Block, S. M.: *Opt. Lett.*, **19**, 1994, p. 930–932.

[20] Selhuber-Unkel, C. et al.: *Nano Lett.*, **8**, 2008, p. 2998–3003.

[21] Brzobohaty, O., et al.: *Sci. Rep. UK*, **5**, 2015, p. 8106.

[22] Arias-Gonzlez, J. R.; M. Nieto-Vesperinas: *J. Opt. Soc. Am. A*, **20**, 2003, 1201–1209.

[23] Nedev, S., et al.: *Nano Lett.*, **11**, 2011, p. 5066–5070.

[24] Kniger, A.; Khler, W.: *ACS Nano*, **6**, 2012, p. 4400–4409.

[25] Svedberg, F. et al.: *Nano Lett.*, **6**, 2006, p 2639–2641.

[26] Messina, E. et al.: *J. Phys. Chem. C*, **115**, 2011, p. 5115–5122.

[27] Fazio B.; D'Andrea C.; Foti A. et al.: *Sci. Rep.*, under decision.

[28] Shemetov, A. A.; Nabiev I.; Sukhanova A.: *ACS Nano*, **6**, 2012 p. 4585–4602.

[29] Zhang, D., et al.: *Nano Lett.*, **9**, 2009, p. 666–671.

[30] Abdul-Salam, V. B., et al.: *Arterioscler. Thromb. Vasc. Biol.*, **30**, 2010, p. 1027–1033.

[31] Cottat M.; DAndrea C. et al.: *J. Phys. Chem. C*, **119**, 2015, p. 15532-15540.

Preparatory studies for the future activities at ELI-NP facility

A.Muoio[1,2], C.Altana[2,3], A. Anzalone[2], F. Cappuzzello[2,3], M. Cavallaro[2], G. Lanzalone[2,4], F. Musumeci[2,3], A. Trifiró[1,5], M. Trimarchi[3,5], S.Tudisco[2]

[1] *Dipartimento di Scienze Matematiche e Informatiche, Scienze Fisiche e Scienze della Terra, viale F. Stagno d'Alcontres 31, Messina, Italy*
[2] *INFN Laboratori Nazionali del Sud, Catania, Italy*
[3] *Dipartimento di Fisica e Astronomia, Universitá di Catania, Catania, Italy*
[4] *Universitá degli Studi di Enna "Kore", Enna, Italy.*
[5] *I.N.F.N., Sezione di Catania, Catania, Italy.*

E-mail: a.muoio@unime.it

Abstract

Performing accurate measurements of nuclear reaction rates of proton and alpha burning processes is essential for the correct understanding of many astrophysical processes. We report the last year activity related to the nuclear physics studies proposed at the future ELI-NP facility.

Keywords: SiC,plasma,laser.

Introduction

A direct measurement of rates and/or cross-sections (S-factors) in laboratory is important to have a better understanding of many astrophysical processes. It is of paramount relevance the measurement of cross-sections at extremely low energetic domains including plasmas effect, i.e. in an environment that under some circumstances and assumptions can be considered as stellar like (for example, for the study of the role played by free/bounded electrons on the Coulombian screening in dense and warm plasmas). NRLP - Nuclear Reaction in Laser Plasma is a project proposed in the past 2013, which aim to perform nuclear studies at the future ELI-NP facility. The main goal is the investigation of nuclear reactions mechanisms and nuclear properties inside plasmas generated trough laser-matter interaction. Such proposal has been widely discussed in the previous activity report 2013-2014 [1] . To conduct such activities, the project aim to take advantage from the excellent and unique performance of the ELI-NP facility and realize an experimental set-up where two colliding plasmas are generated by two laser beams. The use of colliding plasma plumes suitable for nuclear physics studies was proposed few years ago[2]. The idea is to produce ^{13}C, ^{7}Li or ^{11}B plasma through the TNSA (Target Normal Sheath Acceleration)[3] acceleration scheme and use this to impact on a secondary plasma, prepared through the interaction of a laser pulse on a gas jet target (made of ^{4}He, D_2 or ^{3}He). Produced nuclear events can be detected and identified trough a highly segmented detection system for neutrons and charged particles. The highly segmentation is required for the reactions kinematic reconstruction. In these frame during the last year has been conducting several R&D activities related to the several parts of the project. In particular, several experiments devoted to study of the TNSA acceleration schema have been conducted; some test on Silicon Carbide which is the detector candidate for the charged particle identification have been performed. Moreover, numerous tests on scintillation detectors used in laser matter interaction conditions have been performed.

TNSA studies

An experimental campaign aiming at investigating the ions acceleration mechanisms through laser-matter interaction in femtoseconds domain has been carried out at the ILIL facility with a laser intensity of up to 2 10^{19} W/cm^2. A Thomson Parabola Spectrometer (TPS), to obtain the spectra of the ions of the different species accelerated, was used. Several processes involving energy transfer between the laser pulse and target electrons occur, with a significant role played by plasma density gradient set up by the specific laser pulse temporal properties due to Amplified Spontaneous Emission (ASE) and to laser pulse compression. Consequently a population of hot electrons with a mean free path larger than the target thickness is produced. Hence, these electrons can cross the target itself, often subject to strong magnetic fields with complex features de-

pending upon target properties[4-5], setting up an intense electrostatic field due to the charge imbalance between positive ions at rest in the target and the expanding electron sheath[6]. Typically, this field accelerates simultaneously several ion species, originated partly from the bulk target material, but predominantly from the hydrocarbon contaminant layers present on both sides of the target foils. Therefore, such ion sources are typically multi-species (protons, several charge states of carbon and the bulk target elements) and demand spectrometers with adequate charged species discrimination capability.

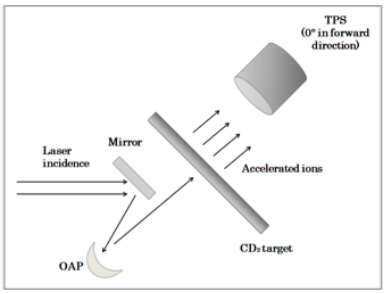

Figure 1: *Sketch of the experimental set-up.*

Detecting and identifying the energy spectra of individual ion species is the key for understanding the underlying acceleration mechanism. In this context, we carried out a systematic experimental investigation to identify the role of target properties in TNSA, with special attention to target thickness and dielectric properties. We used a full range of ion, optical and X-ray diagnostics to investigate laser-plasma interaction and ion acceleration. We focus on the results obtained using the TPS, to characterize ion beams produced in TNSA regime. In the TPS, often used in such experiments, ions with different charge-to-mass ratios are separated into distinct parabolas. This allows to extract information for each ion species when several ions are generated simultaneously in a given solid angle. The working principle, widely described in literature[7-10], is based on parallel electric and magnetic fields acting on a sharply collimated ion beam propagating orthogonally to the fields themselves. The experiments have been performed at the Intense Laser Irradiation Laboratory (ILIL) in Pisa where a Ti:Sapphire laser system, which delivers 40 fs - 800 nm pulses with energy on target up to 400 mJ, is working The ILIL laser pulse exhibits an ASE contrast greater than 10^9 and a ps contrast 10^7 at 10 ps before the peak pulse. The beam is focused on the target at an angle of incidence of 15° using an off-axis parabolic mirror; the corresponding maximum intensity on target was up to 2 x 10^{19} W/cm^2. The target was mounted on a three-axis translational stage system at the center of a 640 mm diameter interaction chamber. Targets consisting of different materials were used. Here we focus on deuterated plastic (CD_2) foil targets of 10μm thickness. TPS was placed in the direction of the normal, with a distance of 129 cm from the target surface to MCP-PH, as shown in Fig. 1. The data analysis provides an estimation of ion energy distributions. By means of TPS calibration it is possible to determine the kinetic energy of different ions (protons and deuterons) distributed along the parabolas and therefore reconstruct the whole spectrum[11]. Fig. 2a shows an example of the TPS spectrogram while Fig. 2b show the proton energy spectrum obtained from data reduction applied to the Fig. 2a. The brightness of the traces is proportional to the number of detected particles.

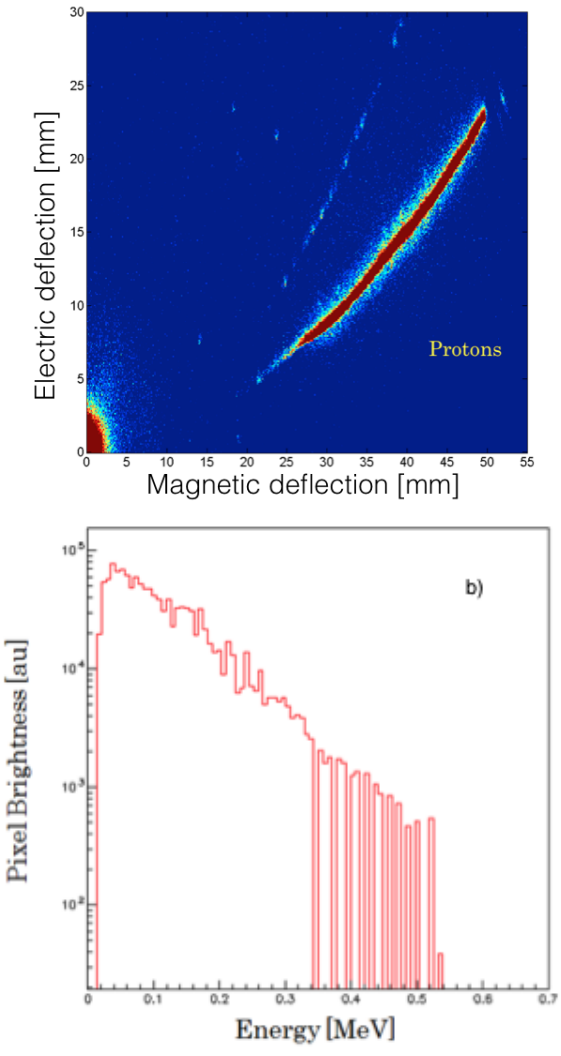

Figure 2: *a) Spectrograms from a 10μm thick CD_2 target. b) Proton spectrum obtained by means of magnetic field.*

The energy spectra of Fig. 2b has been successively fitted assuming an exponen-

tial trend. In such way it is possible to extract the temperature or slope parameter.

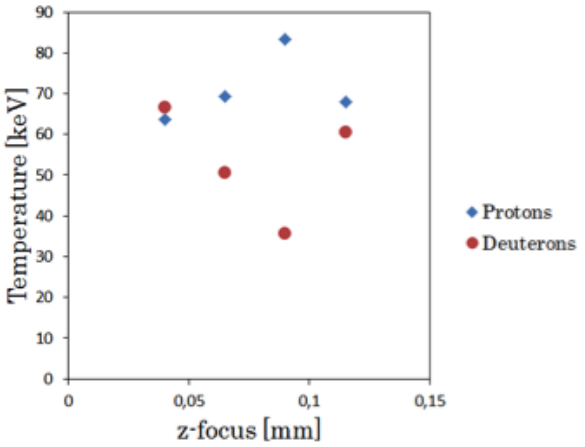

Figure 3: *Temperature of protons (blue diamond) and deuterons (red circle) as function of focus.*

Fig. 3 shows the temperature parameter as a function of the focal position showing that protons and deuterons temperatures exhibit an opposite trend: protons exhibit a maximum corresponding to the best focus where deuterons show a minimum temperature. These preliminary observations clearly show that ion acceleration originates from a complex scenario set by the laser-target interaction conditions. Detailed modeling is currently being carried out to unfold the origin of surface and volume acceleration processes observed here, taking into account the laser target interaction mechanisms as emerging from other measurements including optical and X-ray spectroscopy and optical transition radiation imaging.

SiC studies

Due to its wide gap and strength of its chemical bonds, SIC has been seriously considered as a valid alternative to Si for the production of radiation hard ionizing particle detectors. The leakage current of a p-n junction consists of diffusion current from the quasi-neutral areas and generation current from depletion area[12]. This second term depends essentially on the temperature T and on the energy gap Eg; simply the increasing of Eg from 1.1 eV (Si) up to 3.2 eV (4H-SiC) determines a consistent reduction, about 17 orders of magnitude at room temperature (300K). Silicon Carbide technology offers then an ideal response to such challenges, since it gives the opportunity to cope the excellent properties of silicon detectors (resolution, efficiency, linearity compactness) with a much bigger radiation hardness (up to five orders of magnitude for heavy ions), thermal stability and insensitivity to visible light. R&D activity is mandatory to develop innovative processes, whi]h allows a massive production of thick (>100 μm) and large area (about 1 cm^2) SiC detectors. Following these indications we work with a Monte Carlo simulation with the aim to study ΔE - E configuration (telescope) (with respective thicknesses 100μm and 1000 μm) from the point of view of defects dislocation generated by an ^{18}O at 25 MeV/A. Such telescope cold be used for different application, one of them is detectors wall for charged particles to be used at ELI-NP. For such simulation work we used the SRIM[13] code, which is a collection of packages calculating many features ions motion in the matter. In particular we calculated the number of dislocation generated by ions motion. By using such information it is possible to evaluate the current increment due to radiation damage. In Figure 4, are shown the results of such evaluation, we notice as at high doses irradiation/fluency an increasing of five several order of magnitude in the leakage current is expected. Such increment is not dramatic for a SiC detector, which have a leakage current about five order of magnitude less than a Silicon.

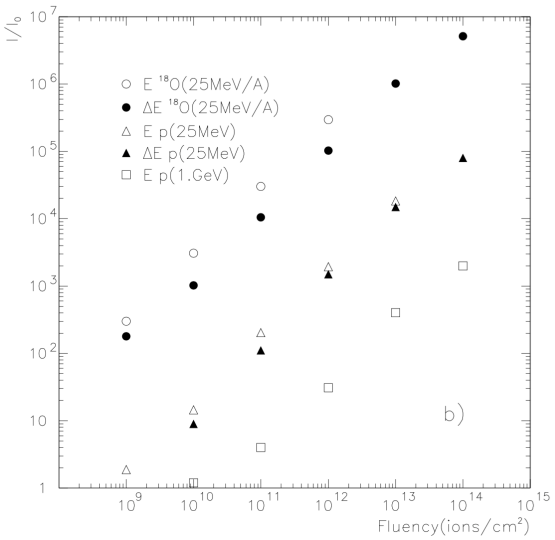

Figure 4: *The figure shows the comparison of Increment of current leakage versus Fluency in SiC for thickness of ΔE and E. Solid symbols are the first stage of the detector (with a thickness of 100μm), while the empty symbols (with a thickness of 1000μm). The following energies has been simulated: oxygen ions at 25 (circle), protons ions at 25 (triangle) and protons ions at 1 (square)*

Moreover the effects of high dose irradiation was experimentally studied, comparing the response of SiC versus a Si detectors. These detectors were irradiated with C$^+$ ions at 740 MeV and at different

Table 1: *Comparison, with several doses, between SiC and Si detectors*

	SiC reverse current[A/cm^3]			Si reverse current[A/cm^3]		
[Volt]	SiCFresh	94kGy	218kGy	SiFresh	94kGy	21kGy
-190	1.910^{-6}	8.610^{-6}	4.510^{-4}	$8.3\ 10^{-5}$	$3.9\ 10^{-4}$	$8.3\ 10^{-5}$
-150	$8.0\ 10^{-7}$	$5.4\ 10^{-6}$	$2.9\ 10^{-4}$	$6.5\ 10^{-6}$	$3.2\ 10^{-4}$	$8.3\ 10^{-5}$
-110	$3.4\ 10^{-7}$	$3.2\ 10^{-6}$	$1.4\ 10^{-4}$	$4.8\ 10^{-6}$	$2.5\ 10^{-4}$	$8.3\ 10^{-5}$
-70	$1.4\ 10^{-7}$	$1.8\ 10^{-6}$	$3.5\ 10^{-5}$	$2.6\ 10^{-6}$	$7.8\ 10^{-5}$	$3.0\ 10^{-5}$
-30	$7.0\ 10^{-8}$	$6.1\ 10^{-7}$	$3.9\ 10^{-7}$	$7.9\ 10^{-7}$	$6.1\ 10^{-5}$	$2.2\ 10^{-5}$
-10	$4.7\ 10^{-8}$	$2.8\ 10^{-7}$	$5.1\ 10^{-8}$	$1.9\ 10^{-7}$	$3.5\ 10^{-5}$	$1.7\ 10^{-5}$

doses. For the experiment we used a standard Si detector of 1 cm^2 of active area and 300 μm thickness and SiC detector which was built growing a 4H-SiC n-type epitaxial layers with a carrier concentration of 1.0 10^{-14}cm^{-3} and a thickness of 80μm on a highly doped n-type ($\sim$7.0 10^{18}cm^3) substrate.Table 1 shows the results of the electrical static characterization before and after the irradiation. Be as Si detector work up to 94kGy dose irradiation while SiC is able to survive up to 218 kGy.

Scintillation detectors studies

Concerning the scintillation detectors, some test has been performed during some test at ILL-INO and at PULSE laboratory in Prague. Aim of this test was to study the response of some scintillator coupled with different readout devices, mainly photomultiplier tube PMT and silicon photo-multiplier SiPM. What has been observed from such test is that the SiPM readout is much less sensitive respect to the PMT devices to the electromagnetic noise typically generated in Laser facility during the pulse irradiation.

References

[1] A.Muoio et al., *University of Messina - Activity Report 2014, ISSN (2038-5889)*. p.61-63.

[2] D. Mascali et al., *Rad. E. and Def. in Sol.* **165** Issue 6-10 (2010) 730., p. 219–222.

[3] S. Tudisco et al.: *Rev. Sci. Instrum.* **87** 02A909 (2016) http://dx.doi.org/10.1063/1.493469.

[4] T. Ceccotti et al., *Phys. Rev. Lett.* **111**, 185001 (2013).

[5] D. Jung et al., *ibid.* **107**, 185001 (2011).

[6] Passoni M et al., *Rev. Sci. Instrum.* vol**55** 1229, (1984).

[7] K. Harres et al., *Rev. Sci. Instrum.* vol.**79** 093306, (2008).

[8] D. Jung et al., *Rev. Sci. Instrum.* vol.**82** 113504, (2011).

[9] J.A. Cobble et al., *Rev. Sci. Instrum.* vol.**82**, 113504, (2011).

[10] Schneider R.F. et al., *J. Appl. Phys.* vol.**57**, 1 (1985).

[11] F. Schillaci et al., *JINST.* vol.**9**, T10003 (2014).

[12] S.M. Sze., *Physics of Semiconductor Devices .* (Ed. Wiley). (1969).

[13] .F.Ziegler et al., *The stopping and range of ions in matter* (Ed. Wiley). (1969).

The InKilsSy experiment: size or isospin effect?

Norella S.[1–2]

[1] *Dipartimento di Scienze Matematiche e Informatiche, Scienze Fisiche e Scienze della Terra, viale F. Stagno d'Alcontres 31, Messina, Italy*
[2] *INFN, Gruppo collegato di Messina, Messina, Italy*

E-mail: snorella@unime.it

Abstract

In this contribution we present the preliminary results of the InKiIsSy experiment, carried out at Laboratori Nazionali del Sud on April 2013. During this experiment the $^{124}Xe(35AMeV) + ^{64}Zn(^{64}Ni)$ reactions were studied, using the multi-detector CHIMERA. Previous experiments have shown differences in the IMF production cross-section between "neutron poor" and "neutron rich" system. This effect could be due to the very different N/Z ratio; but, it also could be related to the different size of the two systems. In order to disentangle isospin effects from size ones, the systems $^{124}Xe + ^{64}Zn(^{64}Ni)$ are being analyzed.

Keywords: Statistical and dynamical emission, Farcos, Isospin, Chimera.

Introduction

Semiperipheral collisions at low energies ($E < 15AMeV$) are characterized by deep inelastic processes. In fact, in the final state of these reactions there is a massive fragment with velocity close to the projectile one, indicated with the term PLF (Projectile-Like Fragment), observed in coincidence with a fragment whose mass is close to the target one, indicated with the term TLF (Target-Like Fragment). These primary fragments are also accompained by the emission of reaction products imputable to the statistical decay of the PLF or TLF. But, already at Fermi energies, these binary reactions begin to be accompained by a copious emission of IMFs (Intermediate Mass Fragments), that are fragments of atomic number $Z \geq 3$. They have a kinematics distribution centred at a velocity intermediate between the velocity of Target-Like Fragment and the one of Projectile-Like Fragment (fig.1), so their emission could not be explained by statistical PLF or TLF decay. The production of these IMFs is due to different reaction mechanisms and different time scales [1], ranging from the fragmentation of the neck to dynamical emission for heavier fragments. The analysis of previous experiments (REVERSE and TIMESCALE), in which the systems $^{124,112}Sn + ^{64,58}Ni$ have been studied, have shown a well-defined chronology: light fragments ($Z < 9$) are specially emitted in fast fragmentation of neck connecting PLF and TLF, while the emission of IMF with $Z \geq 9$ are predominantly emitted at the last stage of neck expansion process and has been associated with the Dynamical Fission mechanism.

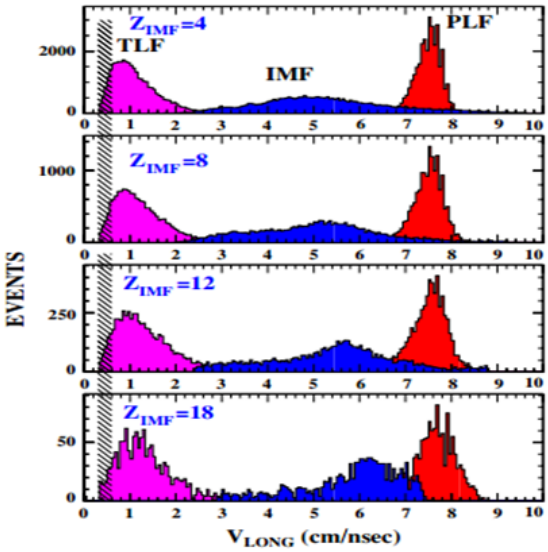

Figure 1: *Longitudinal velocity distribution for Z_{IMF}=4, 8, 12, 18*

In particular, comparing IMFs emission in the neutron rich ($^{124}Sn+^{64}Ni$) and neutron poor ($^{112}Sn+^{58}Ni$) reactions, it has been shown [2, 3] that while the statistical emission has the same probability for both systems, the dynamical fission probability is enhanced up to a factor 1.5-2 in the neutron rich system (fig.2). This effect could be due to the very different N/Z ratio of the two systems. But, some simulations have shown that it could also be related to the different size of the two systems [4, 5].

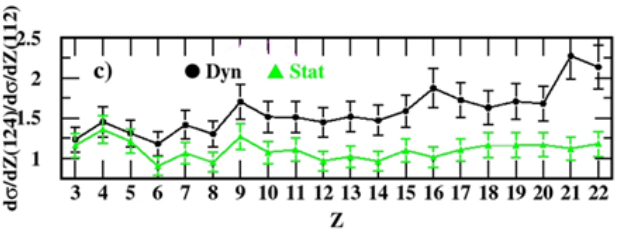

Figure 2: *Ratio of the cross sections of the* $^{124,112}Sn + ^{64,58}Ni$ *systems for dyamical emission (black) and statistical emission (green) as a function of the IMF atomic number*

In order to disentangle effects related to isospin from the ones related to the size of the two interacting systems, a new experimental investigation was carried out at Laboratori Nazionali del Sud.

The InKiIsSy experiment

The InKiIsSy (Inverse Kinematic Isobaric Systems) experiment was carried out to study a projectile/target combination ($^{124}Xe + ^{64}Zn$) having the same mass of the neutron rich system ($^{124}Sn + ^{64}Ni$) and a ratio N/Z close to the value of the neutron poor one ($^{112}Sn + ^{58}Ni$), in order to distinguish isospin effects from size ones. During this experiment the $^{124}Xe + ^{64}Ni$ reaction was also analyzed, in order to compare two systems with same mass and beam but with different N/Z ratio for the target (fig.3).

System	N/Z Projectile	N/Z target	N/Z compound
^{124}Sn+^{64}Ni	1.48	1.29	1.41
^{124}Xe+^{64}Ni	1.30	1.29	1.29
^{124}Xe+^{64}Zn	1.30	1.13	1.24
^{112}Sn+^{58}Ni	1.24	1.07	1.18

Figure 3: *Isospin values for all systems*

Both systems were studied at 35 AMeV beam energy, using CHIMERA multi-detector [6]. It's a 4π detector for charged particles with high resolution and low energy thresholds. It consists of 1192 telescopes grouped into 35 rings in a cylindrical geometry along the beam axis. During this experiment, for the first time, CHIMERA was coupled to a prototype of FARCOS array [7] (fig.4). This is a modular array of telescopes, each of which consists in two double-sided silicon strip detectors (DSSSD) followed by 4 CsI(Tl) crystals. In particular, during this experiment FARCOS telescopes were placed at 25 cm from the target in a 2x2 configuration.

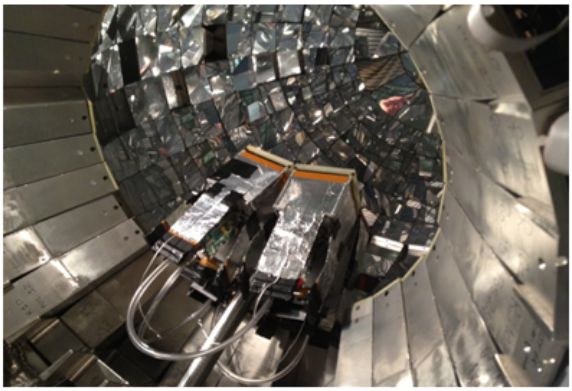

Figure 4: *The InKiIsSy experimental setup*

They subtend the polar angles of $15^o \leq \theta_{lab} \leq 45^o$ and the azimuthal $\Delta\phi \approx 90^o$ in order to detect LCP (Light Charged Particles) and IMFs with higher angular and energy resolution than in CHIMERA.

Preliminary results

The analysis of InKiIsSy experiment is in "progress". Infact, at this time it's limited to particles identified using the $\Delta E - E$ technique in the Silicon-CsI(Tl) Chimera telescopes or PSD tecnique in CsI(Tl). Figure 5 shows the two-dimensional distribution of the fragments for the $^{124}Xe + ^{64}Zn$ reaction as a function of Z of a given fragment and its parallel velocity along the beam axis (fig.5). It's possible to distinguish two main regions, recognized as PLF and IMFs regions.

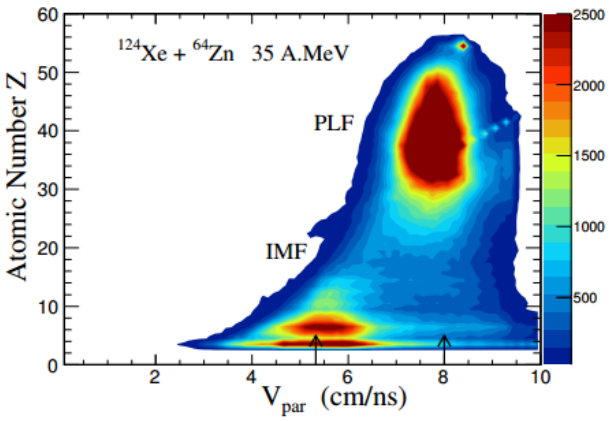

Figure 5: *Distribution of the fragments for the* $^{124}Xe + ^{64}Zn$ *reaction as a function of their atomic number Z and longitudinal velocity*

The projectile-like fragments cover the area corre-

sponding to heavy and relatively fast fragments of atomic number Z approaching the Z of Xe projectile, $Z_{proj} = 54$, and moving with velocities close to projectiles ones. Instead, intermediate mass fragments cover the region of intermediate velocities. They are mostly light fragments, but they can have also larger Z values, up to $Z = 20$.
Binary decay of the PLF, produced in peripheral reactions, were selected assuming that the sum of the charge of the two heaviest fragments $Z_{2F} = Z_1 + Z_2$ was larger than the value of 70% of the projectile charge. In particular, figure 6 shows the v_{par} vs v_{per} Galilean invariant cross-section for the lighter fragment in the reference frame of PLF for two different values of the asymmetry parameter η ($\eta = (Z_1 - Z_2)/(Z_1 + Z_2)$)(fig.6).

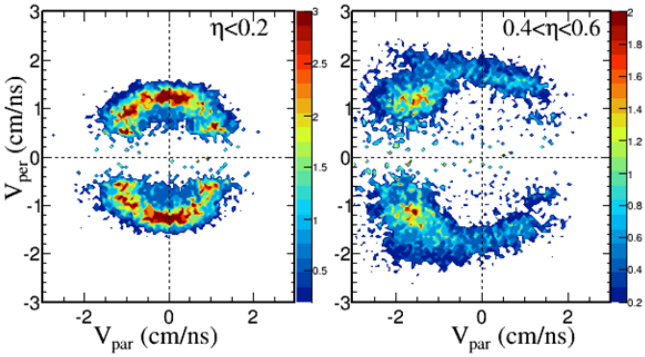

Figure 6: *Invariant cross-sections for the lighter fragment in the reference frame of the PLF for different values of asymmetry parameter*

For symmetry splitting ($\eta < 0.2$) one can see the typical Coulomb ring expected for an equilibrated break-up. But, for large asymmetric splittings ($0.4 < \eta < 0.6$), there is an evident forward-backward asymmetry that indicates a component due to dynamical emission. In order to separate the dynamical emission from the statistical one, the $cos\theta_{prox}$ distribution has been used (fig.7), where θ_{prox} is the angle between direction of the reconstructed PLF and the relative velocity between Z_1 and Z_2 fragments. The statistical contribution has been extrapolated by a "symmetrization" around $cos\theta_{prox} = 0$ of the backward part of the distribution ($cos\theta_{prox} < 0$); while, the dynamical contribution is obtained by subtracting the extrapolated statistical distribution from the total one [8]. In this way, it's possible to estimate the weight of the two components. Figure 8 shows the ratio of dynamical component respect to the total one as a function of IMF atomic number Z for the $^{124}Xe + ^{64}Ni$ and $^{124}Xe + ^{64}Zn$ reactions (fig.8).

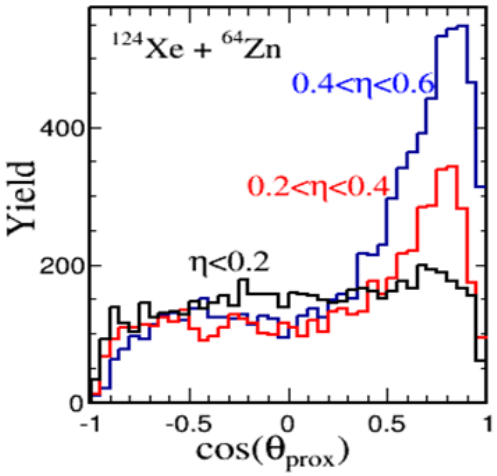

Figure 7: *$Cos\theta_{prox}$ distribution for three different asymmetries η in the binary splitting of the PLF*

As you can see, the dynamical component is larger for the system with a neutron rich target (^{64}Ni). For this reason, considering that the two systems have same mass, it seems that this effect is related to different isospin of the two systems rather than to their initial size. This is a preliminary result; infact the particles of lower energies haven't been identified yet. Data analysis will be completed adding these particles stopped in the silicon detectors and identified in mass and/or charge by Time-of-Flight and Pulse-Shape techniques respectively.

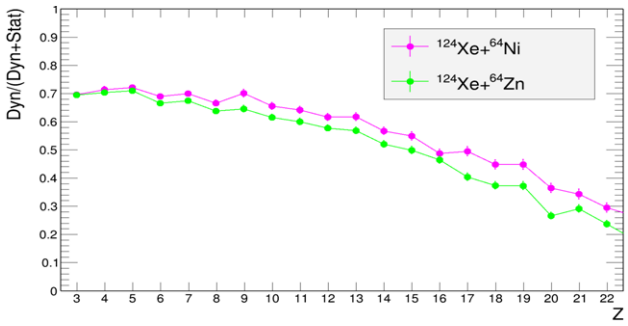

Figure 8: *Ratio of the dynamical component respect to the dynamical+statistical one as a function of IMF atomic number Z for the $^{124}Xe + ^{64}Ni$ and $^{124}Xe + ^{64}Zn$ systems*

Thus, completing analysis, it will be possible to compare these results with those of previous experiment (REVERSE).

Conclusions

In this report, the preliminary results of InKiIsSy experiment were presented. In particular, in pre-

vious experiments, the systems $^{124}Sn +^{64} Ni$ and $^{112}Sn +^{58} Ni$ have been studied in inverse (REVERSE) and direct (TIMESCALE) kinematics at 35 AMeV. The analysis of these two systems has shown that while the statistical IMFs emission assumes the same cross section for the two systems, the dynamical fission probability is enhanced for the neutron rich system. This effect can be related to the different N/Z ratio of the two systems but also to the different size of entrance channel. In order to disentangle these two effects, the $^{124}Xe +^{64} Zn(^{64}Ni)$ are being analyzed at the same bombarding energy. The analysis of this experiment is "in progress" but preliminary results show that this effetc is related to the different isospin of the two systems rather than to their initial size.

References

[1] E. De Filippo *et al.*, Phys. Rev. C**71**, 044602 (2005); *ibidem* Phys. Rev. C**71**, 064604 (2005).

[2] P. Russotto *et al.*, Phys. Rev. C**81**, 064605 (2010).

[3] P. Russotto *et al.*, Phys. Rev. C**91**, 014610 (2015).

[4] M. Papa *et al.*, Procs of IWM2007.

[5] M. Papa *et al.*, PRC75, 054616 (2007).

[6] A. Pagano *et al.*, Nucl. Phys. A **734**, 504 (2004).

[7] E.V. Pagano *et al.*, Procs of NN2015.

[8] F. Bocage *et al.*, Nucl. Phys. A **676**, 391 (2000).